Article

Product Bound Structures of the Soluble Methane Monooxygenase Hydroxylase from *Methylococcus capsulatus* (Bath): Protein Motion in the □-Subunit

Matthew H. Sazinsky, and Stephen J. Lippard

J. Am. Chem. Soc., **2005**, 127 (16), 5814-5825• DOI: 10.1021/ja044099b • Publication Date (Web): 02 April 2005

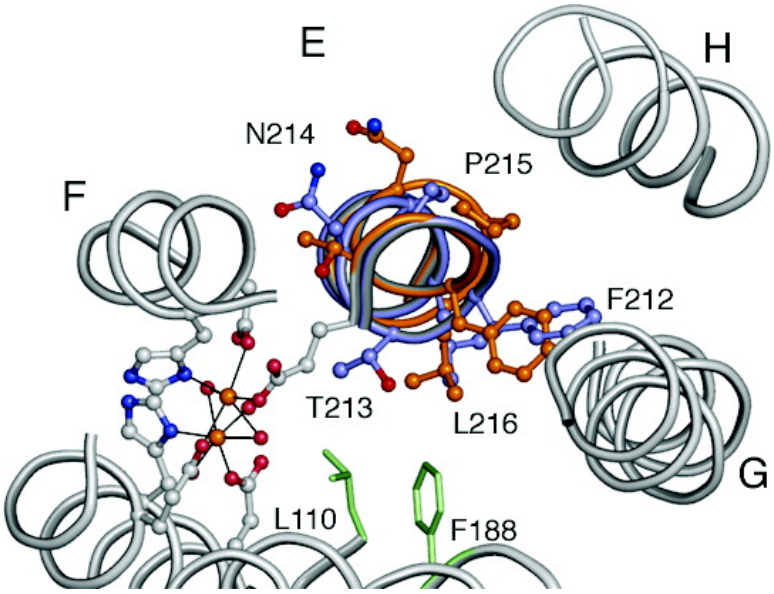

More About This Article

Additional resources and features associated with this article are available within the HTML version:

- Supporting Information
- Links to the 4 articles that cite this article, as of the time of this article download
- Access to high resolution figures
- Links to articles and content related to this article
- Copyright permission to reproduce figures and/or text from this article

View the Full Text HTML

J|A|C|S
ARTICLES
Published on Web 04/02/2005

Product Bound Structures of the Soluble Methane Monooxygenase Hydroxylase from *Methylococcus capsulatus* (Bath): Protein Motion in the α-Subunit

Matthew H. Sazinsky and Stephen J. Lippard*

Contribution from the Department of Chemistry, Massachusetts Institute of Technology, Cambridge, Massachusetts 02139

Received September 28, 2004; E-mail: lippard@lippard.mit.edu

Abstract: The soluble methane monooxygenase hydroxylase (MMOH) α-subunit contains a series of cavities that delineate the route of substrate entrance to and product egress from the buried carboxylate-bridged diiron center. The presence of discrete cavities is a major structural difference between MMOH, which can hydroxylate methane, and toluene/*o*-xylene monooxygenase hydroxylase (ToMOH), which cannot. To understand better the functions of the cavities and to investigate how an enzyme designed for methane hydroxylation can also accommodate larger substrates such as octane, methylcubane, and *trans*-1-methyl-2-phenylcyclopropane, MMOH crystals were soaked with an assortment of different alcohols and their X-ray structures were solved to 1.8−2.4 Å resolution. The product analogues localize to cavities 1−3 and delineate a path of product exit and/or substrate entrance from the active site to the surface of the protein. The binding of the alcohols to a position bridging the two iron atoms in cavity 1 extends and validates previous crystallographic, spectroscopic, and computational work indicating this site to be where substrates are hydroxylated and products form. The presence of these alcohols induces perturbations in the amino acid side-chain gates linking pairs of cavities, allowing for the formation of a channel similar to one observed in ToMOH. Upon binding of 6-bromohexan-1-ol, the π helix formed by residues 202−211 in helix E of the α-subunit is extended through residue 216, changing the orientations of several amino acid residues in the active site cavity. This remarkable secondary structure rearrangement in the four-helix bundle has several mechanistic implications for substrate accommodation and the function of the effector protein, MMOB.

Introduction

Microorganisms play a significant role in bioremediation as demonstrated by their ability both to cleanse environments contaminated with such xenobiotics as oil spills, haloalkanes, and aromatics and to use these hydrocarbon substrates as a source of carbon and energy.[1−3] Non-heme diiron bacterial multicomponent monooxygenases (BMMs),[4,5] including the soluble methane monooxygenase, four-component alkene/aromatic monooxygenase, phenol hydroxylase, and alkene monooxygenase subfamilies, are in part responsible for the chemically challenging transformations performed by the microorganisms harboring these enzymes. Only members of the soluble methane monooxygenase (sMMO) subfamily, which include methane, butane, and related monooxygenases, can hydroxylate alkanes. This unique property has garnered much attention among those interested in C−H bond activation chemistry and in bioengineering these enzymes for synthetic and environmental applications.

Soluble methane monooxygenase is a three-component enzyme system comprising a 251-kDa hydroxylase of the form $\alpha_2\beta_2\gamma_2$ (MMOH), a 16-kDa cofactorless protein (MMOB) that couples electron transfer with dioxygen activation, and a 38-kDa [2Fe−2S]- and FAD-containing reductase (MMOR).[6] At a carboxylate-bridged diiron center housed within a four-helix bundle in each of the MMOH α-subunits, both diiron(III) peroxo and high-valent di(μ-oxo)diiron(IV) intermediates convert hydrocarbon substrates either to alcohols or epoxides (eqs 1 and 2).[6−8] For these reactions to take place, several substrates, including the hydrocarbon, O_2, $2e^-$, and $2H^+$, must access the diiron center when the MMOR and MMOB components are bound to the hydroxylase.[9] For efficient activity, the enzyme must precisely time these interactions as well as facilitate the extrusion of products from the active site through noninterfering pathways. To account for the differences in polarity between

$$CH_4 + NADH + H^+ + O_2 \longrightarrow CH_3OH + NAD^+ + H_2O \quad (1)$$

$$R\text{-}CH{=}CH_2 + NADH + H^+ + O_2 \longrightarrow \text{(epoxide)} + NAD^+ + H_2O \quad (2)$$

the hydrophobic and polar substrates and products, it has been

* Corresponding author. E-mail: lippard@mit.edu.

(1) Hanson, R. S.; Hanson, T. E. *Microbiol. Rev.* **1996**, *60*, 439−471.
(2) Sullivan, J. P.; Dickinson, D.; Chase, H. A. *Crit. Rev. Microbiol.* **1998**, *24*, 335−373.
(3) Pieper, D. H.; Reineke, W. *Curr. Opin. Biotech.* **2000**, *11*, 262−270.
(4) Leahy, J. G.; Batchelor, P. J.; Morcomb, S. M. *FEMS Microbiol. Rev.* **2003**, *27*, 449−479.
(5) Notomista, E.; Lahm, A.; Di Donato, A.; Tramontano, A. *J. Mol. Evol.* **2003**, *56*, 435−445.
(6) Merkx, M.; Kopp, D. A.; Sazinsky, M. S.; Blazyk, J. L.; Müller, J. M.; Lippard, S. J. *Angew. Chem., Int. Ed. Engl.* **2001**, *40*, 2783−2807.
(7) Beauvais, L. G.; Lippard, S. J. *J. Am. Chem. Soc.* **2005**, *127*, in press.
(8) Valentine, A. M.; Stahl, S. S.; Lippard, S. J. *J. Am. Chem Soc.* **1999**, *121*, 3876−3887.

10.1021/ja044099b CCC: $30.25

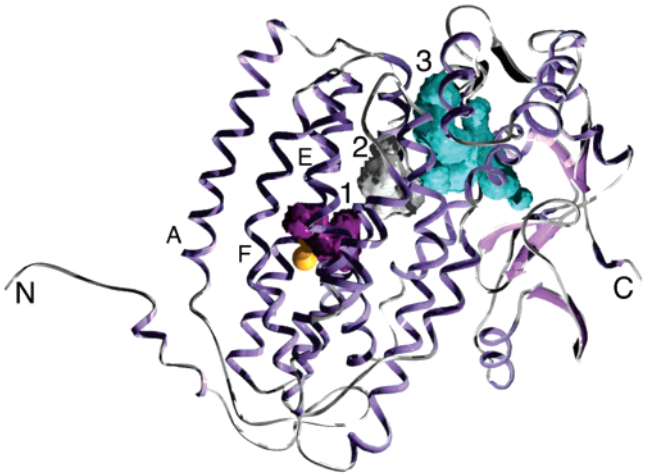

Figure 1. The α-subunit of MMOH depicting the hydrophobic cavities. The diiron center is represented as orange spheres. Cavities 1−3, helices A, E, and F, and the N- and C-termini are labeled.

proposed that sMMO may invoke different routes through MMOH for their entry and exit.[10]

Several hydrophobic cavities in the MMOH α-subunit have been identified, of which three extend from the active site pocket, cavity 1, through the core of the protein to the surface (Figure 1).[10,11] In two different crystal forms of MMOH, Leu-110, which sits at the interface between cavities 1 and 2,[12] adopts alternate rotamer conformations and was therefore proposed to gate substrate passage between these two cavities.[11,12] Subsequently, it was demonstrated that small halogenated alkanes and xenon can bind in cavities 2 and 3,[10] reinforcing the hypothesis that they delineate an essential pathway for substrate entrance into the diiron center other than by direct diffusion through the four-helix bundle in which the active site is held. Further evidence in support of the postulated hydrocarbon route was the discovery of a 40 Å long channel in the related enzyme toluene/*o*-xylene monooxygenase hydroxylase (ToMOH) that traces a path identical to that of the MMOH cavities.[13] This finding suggested that all multicomponent monooxygenases deliver substrates and extrude products along this pathway.

The remarkable bioremediating capabilities of some methanotrophs derive from their ability to hydroxylate, and thereby consume, a variety of different substrates, which include branched, cyclic, aromatic, and linear hydrocarbons of up to C8 in length.[14−16] Given the size of some of these compounds, it is difficult to imagine how an enzyme that is designed for processing small substrates such as CH_4 and O_2 can accommodate molecules as large as octane, methylcubane, and *trans*-1-methyl-2-phenylcyclopropane in the same manner.[14,17−19] For sMMO to act on these alternative substrates, its active site must be relatively flexible, yet specific enough to guide and orient them toward the diiron center for hydroxylation. If these larger substrates diffuse through the cavities to gain access to the active site, significant rearrangement of key residue side chains must occur.

In the present work, we determined crystal structures of MMOH with bound aromatic and halogenated alcohols of C2−C8 in length in order to investigate how the enzyme accommodates so many different hydrocarbon compounds and to track the likely route of product passage from the diiron center. These molecules bind in cavities 1−3 of MMOH, alter the conformations of key residues separating the three cavities, and in one case induce novel secondary structure rearrangements in helix E, a component of the four-helix bundle that contributes several key amino acids to the active site pocket. These findings reveal how sMMO can hydroxylate large substrates and strongly suggest that substrates as well as products can move through MMOH along the same path. The unprecedented folding rearrangements in helix E also reveal one way in which MMOB could induce structural changes in MMOH to influence its reactivity.

Experimental Section

Crystallization of MMOH and Small Molecule Soaks. MMOH was purified as described previously.[20,21] Ferrozine assays confirmed the presence of 3.8 ± 0.1 Fe/MMOH and propylene oxidation, followed by measuring NADH consumption, confirmed the activity of the enzyme at 45 °C to be ∼250−300 nmol min^{-1} mg^{-1} (50−60 s^{-1}).[9] Form II crystals were obtained at 4 °C by using the sitting drop vapor diffusion method under conditions similar to those described previously.[11,22] Well solutions contained 160 mM MOPS, pH 7.0, 350 mM $CaCl_2$, 10% PEG 8000 (w/w), and 0.015% NaN_3. Crystallization drops were formed by combining 3 μL of a 50 μM MMOH solution in 25 mM MOPS, pH 7.0, with 1.5 μL of well solution and 1.5 μL of an MMOH microseed stock solution (50 mM MOPS, pH 7.0, 220 mM $CaCl_2$, 10% (w/w) PEG 8000, and 25% (v/v) glycerol). The cryo-solution for crystal freezing contained the well solution plus 25% glycerol. Small molecules were soaked into MMOH crystals by bathing them in a cryo-solution containing various halo alcohols. Soaking times and small molecule concentrations depended upon crystal stability and are listed in Table 1.

Data Collection and Model Refinement. Data sets were collected at SSRL on beam lines 7-1, 9-1, and 11-1 at 100 K with 0.5° oscillations over a 100−120° rotation of the crystal about the φ axis. The program MOSFLM was used to determine a collection strategy and the HKL suite of programs was used to index and scale the data.[23,24] Molecular replacements and refinement were performed by using CNS and XtalView.[25,26] The final crystal and model statistics are presented in Table 1. The different product bound hydroxylase structures closely resemble those described previously.[10,12,27] The MMOH α-subunit

(9) Gassner, G. T.; Lippard, S. J. *Biochemistry* **1999**, *38*, 12768−12785.
(10) Whittington, D. A.; Rosenzweig, A. C.; Frederick, C. A.; Lippard, S. J. *Biochemistry* **2001**, *40*, 3476−3482.
(11) Rosenzweig, A. C.; Brandstetter, H.; Whittington, D. A.; Nordlund, P.; Lippard, S. J.; Frederick, C. A. *Proteins* **1997**, *29*, 141−152.
(12) Rosenzweig, A. C.; Frederick, C. A.; Lippard, S. J.; Nordlund, P. *Nature* **1993**, *366*, 537−543.
(13) Sazinsky, M. H.; Bard, J.; Di Donato, A.; Lippard, S. J. *J. Biol. Chem.* **2004**, *279*, 30600−30610.
(14) Colby, J.; Stirling, D. I.; Dalton, H. *Biochem. J.* **1977**, *165*, 395−402.
(15) Dalton, H. *Adv. Appl. Microbiol.* **1980**, *26*, 71−87.
(16) Green, J.; Dalton, H. *J. Biol. Chem.* **1989**, *264*, 17698−17703.
(17) Choi, S.-Y.; Eaton, P. E.; Kopp, D. A.; Lippard, S. J.; Newcomb, M.; Shen, R. *J. Am. Chem. Soc.* **1999**, *121*, 12198−12199.
(18) Valentine, A. M.; LeTadic-Biadatti, M.-H.; Toy, P. H.; Newcomb, M.; Lippard, S. J. *J. Biol. Chem.* **1999**, *274*, 10771−10776.
(19) Liu, K. E.; Johnson, C. C.; Newcomb, M.; Lippard, S. J. *J. Am. Chem. Soc.* **1993**, *115*, 939−947.
(20) Fox, B. G.; Froland, W. A.; Dege, J. E.; Lipscomb, J. D. *J. Biol. Chem.* **1989**, *264*, 10023−10033.
(21) Willems, J.-P.; Valentine, A. M.; Gurbiel, R.; Lippard, S. J.; Hoffman, B. M. *J. Am. Chem. Soc.* **1998**, *120*, 9410−9416.
(22) Sazinsky, M. H.; Merkx, M.; Cadieux, E.; Tang, S.; Lippard, S. J. *Biochemistry* **2004**, *43*, 16263−16276.
(23) Leslie, A. G. W. *Joint CCP4+ESF-EAMCB Newslett. Prot. Crystallogr.* **1992**, *26*.
(24) Otwinowski, Z.; Minor, W. *Methods Enzymol.* **1997**, *276*, 307−326.
(25) Brünger, A. T.; Adams, P. D.; Clore, G. M.; Delano, W. L.; Gros, P.; Grosse-Kunstleve, R. W.; Jiang, J.-S.; Kuszewski, J.; Nilges, N.; Pannu, N. S.; Read, R. J.; Rice, L. M.; Simonson, T.; Warren, G. L. *Acta Cryst., Sect. D* **1998**, *54*, 905−921.
(26) McRee, D. E. *J. Struct. Biol.* **1999**, *125*, 156−165.

Table 1. Data Collection and Refinement Statistics

	2-Br-ethan-1-ol	3-Cl-propan-1-ol	3-Br-3-buten-1-ol	6-Br-hexan-1-ol	8-Br-octan-1-ol	phenol	4-F-phenol	4-Br-phenol	6-Br-hexan-1-ol reduced
soaking time (min)	20	20	10	15	15	20	60	60	60
soaking concentration	100 mM	20 mM	10 mM	saturating	saturating	10 mM	60 mM	10 mM	saturating
				Data Collection					
beamline	SSRL 7-1	SSRL 11-1	SSRL 11-1	SSRL 11-1	SSRL 11-1	SSRL 11-1	SSRL 9-1	SSRL 9-1	SSRL 9-1
wavelength (Å)	1.08	1.00	1.00	1.00	1.00	1.00	0.979	0.979	0.979
space group	$P2_12_12_1$	$P2_12_12_1$	$P2_12_12_1$	$P2_12_12_1$	$P2_12_12_1$	$P2_12_12_1$	$P2_12_12_1$	$P2_12_12_1$	$P2_12_12_1$
unit cell dimensions (Å)									
a	*71.28*	*70.88*	*70.47*	*70.63*	*70.41*	*71.18*	*71.18*	*71.48*	*71.05*
b	*171.53*	*171.49*	*171.93*	*171.86*	*171.08*	*171.55*	*171.49*	*171.85*	*171.60*
c	221.424	221.05	220.50	220.62	220.62	221.09	221.30	221.42	220.41
resolution range (Å)	30−1.95	30−2.0	30−2.4	30−1.8	30−2.0	30−1.96	30−2.3	30−2.3	30−2.5
total reflections	798,442	776,874	403,659	842,480	674,046	787,803	462,856	458,493	506,562
unique reflections	197,561	180,877	102,181	244,201	176,340	193,972	119,593	119,660	92,629
completeness (%)[a]	99.8 (98.2)	99.4 (97.7)	96.7 (81.7)	98.3 (93.8)	97.3 (83.7)	99.7 (99.4)	99.3 (99.8)	98.3 (98.2)	98.2 (86.9)
$I/\sigma(I)$	13.1 (2.7)	14.2 (4.0)	15.1 (3.2)	16.8 (2.8)	16.2 (4.1)	12.8 (3.2)	17.6 (4.2)	16.6 (4.1)	14.7 (3.3)
R_{sym} (%)[b]	8.2 (46.1)	7.9 (36.4)	7.9 (34.6)	9.0 (32.6)	7.4 (26.2)	7.4 (40.4)	9.0 (38.1)	9.0 (36.8)	5.8 (46.4)
Refinement									
R_{cryst} (%)[c]	19.9	19.9	20.5	22.5	19.9	20.0	19.4	19.9	23.5
R_{free} (%)[d]	23.1	22.7	25.9	25.1	23.0	22.9	22.9	24.5	28.4
number of atoms	18640	18646	17846	18548	18290	18453	18303	18303	17344
protein	17317	17317	17317	17324	17320	17317	17327	17327	17231
water	1269	1283	465	1140	1153	1123	956	956	95
rmsd bond length (Å)	0.0055	0.0068	0.0062	0.0056	0.0054	0.0055	0.0059	0.0063	0.0079
rmsd bond angle (deg)	1.16	1.33	1.20	1.17	1.18	1.18	1.16	1.20	1.30
average *B*−value (Å^2)	26.5	30.3	40.4	36.2	37.1	25.1	41.3	40.9	66.4
PDB ID	1XVG	1XVF	1XVE	1XVB	1XVC	1XU5	1XVD	1XU3	

[a] Values in parentheses are for the highest resolution shell. [b] $R_{sym} = \sum_i\sum_{hkl} |I_i(hkl) - \langle|I(hkl)\rangle|/\sum_{hkl}\langle I(hkl)\rangle$, where $I_i(hkl)$ is the *ith* measured diffraction intensity and $\langle I(hkl)\rangle$ is the mean of the intensity for the Miller index (*hkl*). [c] $R_{cryst} = \sum_{hkl}||F_o(hkl)| - |F_c(hkl)||/\sum_{hkl}|F_o(hkl)|$. [d] $R_{free} = R_{cryst}$ for a test set of reflections (5% in each case).

Table 2. Halogenated Alcohol Binding Sites in MMOH[a]

compound	location	*B*-value (Å^2)	compound	location	*B*-value (Å^2)
2-Br-ethan-1-ol			3-Cl-propan-1-ol		
1	α1, cavity 1	42.5	1	α1, cavity 1	63.1
2	α1, cavity 2	44.5	2	α1, cavity 2	46.6
3	α1, cavity 3	50.4	3	α1, cavity 3	28.2
4	α2, cavity 1	43.3	4	α2, cavity 1	45.2
5	α2, cavity 2	43.9	5	α2, cavity 2	40.6
6	α2, cavity 3	41.8	6	α2, cavity 3	20.2
7	α1/β1 interface	32.9	7	α2/β1 interface	53.3
8	β1/β2, interface	58.1	3-Br-3-butenol		
9	β2/β1, interface	67.6	1	α1, cavity 1	82.8
10	α2/β2 interface	36.2	2	α1, cavity 2	101.3
11	β1, surface	55.9	3	α1, cavity 3	72.4
12	β2, surface	77.2	4	α2, cavity 1	109.5
6-Br-hexan-1-ol			5	α2, cavity 2	106.3
1	α1, cavity 1	61.5	6	α2, cavity 3	64.6
2	α1, cavity 2	60.0	7	α1/β2 interface	93.7
3	α1, cavity 3	47.5	8	α2/β1 interface	86.8
4	α2, cavity 1	68.2	9	α1, surface	97.8
5	α2, cavity 2	57.3	10	α2 on γ2 side	89.1
6	α2, cavity 3	44.0	8-Br-octan-1-ol		
7	α1/β2 interface	85.5	1	α1, cavity 3	49.5
8	α2/β1 interface	61.5	2	α1, cavity 2+3	73.4
9	α2, surface	83.4	3	α1 on γ1 side	77.2
10	α1/β1 N-term	74.9	4	α2 on γ2 side	63.0
11	α2/β2 N-term	71.9	4-Br-phenol		
12	α1 on g1 side	81.9	1	α1, cavity 3	49.8
13	α2 on g2 side	62.8	2	α2, cavity 3	57.5

[a] α1, α2, β1, β2, γ1, and γ2 refer to the subunits of protomers 1 and 2. Occupancies are presented for just the bromine and chlorine atoms.

cavities were calculated by using a 1.4 Å radius water probe in Swiss-PDB Viewer.[28]

Results

Alcohol Binding to MMOH. Several ω-halo alcohols were soaked into crystals of MMOH. The halogen atom was used to differentiate the alcohol group from the methyl group at the opposite end of the linear hydrocarbon chain in the electron density maps. The various locations of each of the soaked halogenated molecules are described in Table 2 and depicted in Figure S1 (Supporting Information).

At the active site (cavity 1), 2-bromoethan-1-ol, 3-chloropropan-1-ol, 3-bromo-3-buten-1-ol, and 6-bromohexan-1-ol bind to a position bridging the two iron atoms (Figure 2). For 6-bromohexan-1-ol, electron density is available for only the bromine atom and the first few carbons after the alcohol moiety. 8-Bromooctan-1-ol and the aromatic alcohols were not located in this cavity. Higher *B*-values and weaker electron density are observed, in general, as the size of the bound alcohol in cavity 1 increases (Table 2).

All of the nonaromatic halo alcohols bind to cavities 2 and 3 with the exception of 8-bromooctan-1-ol, which spans these cavities in one protomer and binds only to cavity 3 in the other. Electron density for 8-bromooctan-1-ol is available primarily

(27) Whittington, D. A.; Sazinsky, M. H.; Lippard, S. J. *J. Am. Chem. Soc.* **2001**, *123*, 1794−1795.
(28) Guex, N.; Peitsch, M. C. *Electrophoresis* **1997**, *18*, 2714−2723.

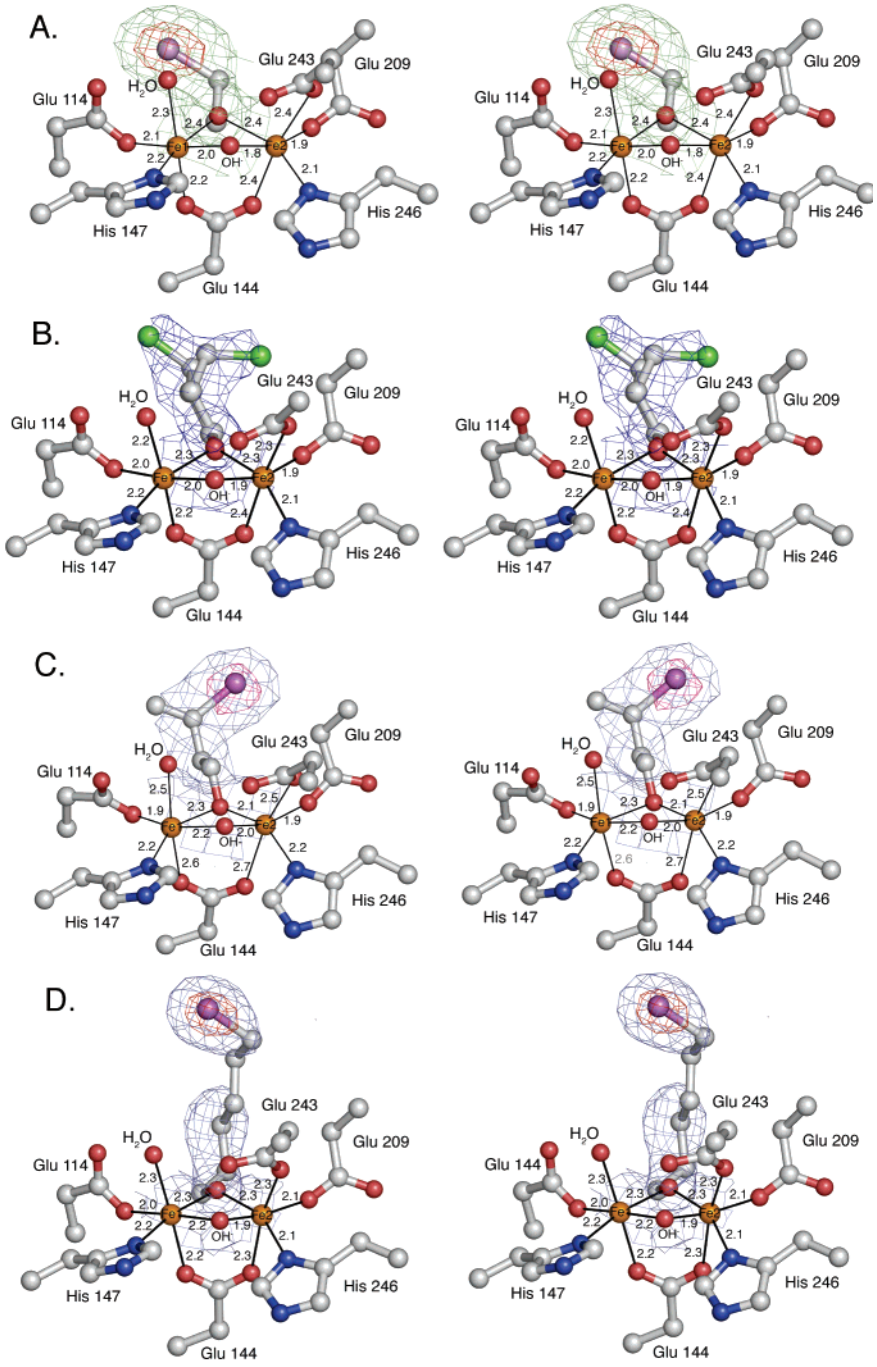

Figure 2. MMOH active sites depicting bound alcohols in stereoviews. $|F_o| - |F_c|$ sa-omit maps contoured to 3 σ (blue/green) and 8 σ (red) are drawn around the bound (A) 2-bromoethan-1-ol, (B) 3-chloropropan-1-ol, (C) 3-bromo-3-buten-1-ol, and (D) 6-bromohexan-1-ol molecules. The active sites from the second protomer appear similar. The atoms are colored by type, where gray is carbon, red is oxygen, blue is nitrogen, orange is iron, green is chlorine, and purple is bromine.

for the bromine atom and the first few attached carbon atoms. Density for the remainder of the chain is absent, probably reflecting positional disorder. In contrast, the electron density is present for almost all of the 2-bromoethan-1-ol, 3-chloropropan-1-ol, 3-bromo-3-buten-1-ol, and 6-bromohexan-1-ol atoms in cavities 2 and 3.

Aromatic compounds such as benzene and nitrobenzene are sMMO substrates and their product alcohols, phenol and *p*-nitrophenol, bind to the diiron center as demonstrated by UV−vis and EPR spectroscopic investigations.[29−32] It was therefore unexpected that, in the structures of MMOH crystals soaked in phenol, 4-fluorophenol, and 4-bromophenol, electron density for these molecules was detected only in cavity 3. *p*-Nitrophenol also binds exclusively to cavity 3 (data not shown). The different aromatics were used to examine the effects of variable polarity

(29) Andersson, K. K.; Froland, W. A.; Lee, S.-K.; Lipscomb, J. D. *New J. Chem.* **1991**, *15*, 411−415.
(30) Liu, K. E.; Valentine, A. M.; Wang, D. L.; Huynh, B. H.; Edmondson, D. E.; Salifoglou, A.; Lippard, S. J. *J. Am. Chem Soc.* **1995**, *117*, 10174−10185.
(31) Davydov, R.; Valentine, A. M.; Komar-Panicucci, S.; Hoffman, B. M.; Lippard, S. J. *Biochemistry* **1999**, *38*, 4188−4197.
(32) Andersson, K. K.; Elgren, T. E.; Que, L.; Lipscomb, J. D. *J. Am. Chem. Soc.* **1992**, *114*, 8711−8713.

Table 3. Cavity Connectivity and Side-Chain Movements in Product-Soaked MMOH Crystal Structures

alcohol	cavity connectivity protomer 1	cavity connectivity protomer 2	α-subunit backbone perturbations	cavity side chains with altered positions[a]
2-bromoethan-1-ol	1+2+3	1+2+3		Cav1: L110, F188, T213, I217 Cav2: L289, M184
3-chloropropan-1-ol	2+3	2+3		Cav1: L110, F188 Cav2: L289, M184
3-bromo-3-buten-1-ol	2+3	2+3		Cav1: L110, F188 Cav2: L289, M184
6-bromohexan-1-ol	2+3	2+3	residues 212-216	Cav1: L110, F188, I217, F212-L216 Cav2: F282, L286, L289, M184
8-bromooctan-1-ol[b]	1+2+3	2+3		Cav1: L110, F188, T213 Cav2: L289, M184
4-fluorophenol	none	none		Cav1: L110 Cav2: M184
4-bromophenol	none	none		Cav1: L110, T213 Cav2: M184
Phenol	none	none		Cav1: L110 Cav2: M184

[a] Based on comparison to $MMOH_{ox}$ crystal form II α-subunits. [b] Designates product that spans cavities 2 and 3.

Table 4. Fe-Fe and Fe−O Bridge Ligand Bond Distances in Different Product-Bound Structures[a]

	H_{ox} (PDB code 1MHY)	methanol (PDB code 1FZ6)	ethanol (PDB code 1FZ7)	2-Br-ethan-1-ol	3-Cl-propan-1-ol	3-Br-buten-3-ol	6-Br-hexan-1-1ol
Fe1−Fe2	3.0	3.0	3.2	3.1	3.2	3.2	3.1
				3.2	3.1	3.0	3.1
Fe1−ROH	2.1 (OH^-)	2.1	2.2	2.4	2.3	2.3	2.3
				2.2	2.1	2.1	2.2
Fe2−ROH	2.2	2.1	2.6	2.4	2.3	2.1	2.3
				2.4	2.5	2.0	2.3
Fe1−OH	1.7	1.9	2.1	1.9	2.0	2.2	2.2
				2.0	1.9	2.3	2.2
Fe2−OH	2.0	1.9	1.8	1.8	1.9	2.0	1.9
				2.0	1.8	2.1	1.8

[a] All distances are in Å. Distances from both protomers are listed from those actives sites in which an alcohol was bound. Values are reported for coordinates published in the protein database (PDB) or from this work.

and pK_a of the −OH group on binding to the active site, but this approach was not fruitful.

The halogenated alcohols also bind to several regions on the surface of MMOH, as well as the α/β and β/β subunit interfaces, N-terminal portions of the β-subunit, and the α-subunit near the α/γ interface. Figure S1 and Tables 2 and 3 report where these different molecules bind, which in general tend to be hydrophobic crevices and niches within the protein. None of the bound surface alcohols are positioned within close proximity to a potential cavity opening or near the diiron center. Dibromomethane and iodoethane were reported previously to bind to similar locations on the MMOH surface,[10] suggesting these sites are adventitious and most likely not relevant to the catalytic function of sMMO.

Product Binding to Cavity 1. In each of the 2-bromoethan-1-ol, 3-chloropropan-1-ol, 3-bromo-3-buten-1-ol, and 6-bromohexan-1-ol structures, the hydroxyl group of the alcohol displaces the bridging OH^- or $H_3O_2^-$ ion facing the hydrophobic pocket in cavity 1 and binds to the diiron center in either a bridging, or in some protomers, an asymmetric, or semi-bridging, fashion (Figure 2).[33] On average, the distances from Fe1 and Fe2 to the alcohol oxygen atom are each ∼2.3 Å (Table 4). Methoxy- and ethoxy-bridged high-spin diiron(III) centers typically have bridging Fe−O bond distances between 1.9 and 2.1 Å, according to results for model complexes deposited in the Cambridge Structural Database. In the methanol-bound structure of MMOH these distances were each 2.1 Å.[27] The longer bond distances observed for the various product-soaked structures suggest that the alcohol rather than the alkoxide species may be coordiinated to the diiron(III) center, but the resolution of the structures is not significantly high to allow for a definitive assignment. The coordination sphere around the irons is relatively unperturbed and identical to that of oxidized MMOH and its methanol and ethanol bound forms.[27]

In all cases, the bound halogenated alcohols extend from the diiron center bridging position toward the back of cavity 1 either near Leu-110 and Phe-188, which serve as the gates to cavity 2, or Phe-192, Gly-208, and Leu-204, which form a niche on the Fe2 side of the active site pocket. In some cases, depending upon the length of the product analogue, the chlorine and bromine atoms are positioned over the aromatic rings of either Phe-188 or Phe-192. The chlorine atom of 3-chloropropan-1-ol is disordered, binding to both of the sites mentioned above, as evidenced by the forked electron density in one of the two active sites (Figure 2B). The bromine atom of 6-bromohexan-1-ol is situated at the roof of the active site cavity and occupies the position of Thr-213 in $MMOH_{ox}$, which has moved because of structural rearrangements that occur in helix E (see below) (Figures 4 and 5). The presence of these small alcohols in cavity 1 perturbs the rotameric conformations of Ile-217, Leu-110, Phe-188, and Thr-213 (Figure 3A). Leu-110 adopts different conformations in the two different crystal forms of MMOH.[11] The presence of the halo alcohol substrates in crystal form II induces this residue to adopt a conformation similar to that observed in form I MMOH crystals. The phenyl ring of Phe-188, which comprises part of the "leucine gate," shifts to the left or right in the different MMOH structures, seemingly in

(33) Whittington, D. A.; Lippard, S. J. *J. Am. Chem Soc.* **2001**, *123*, 827−838.

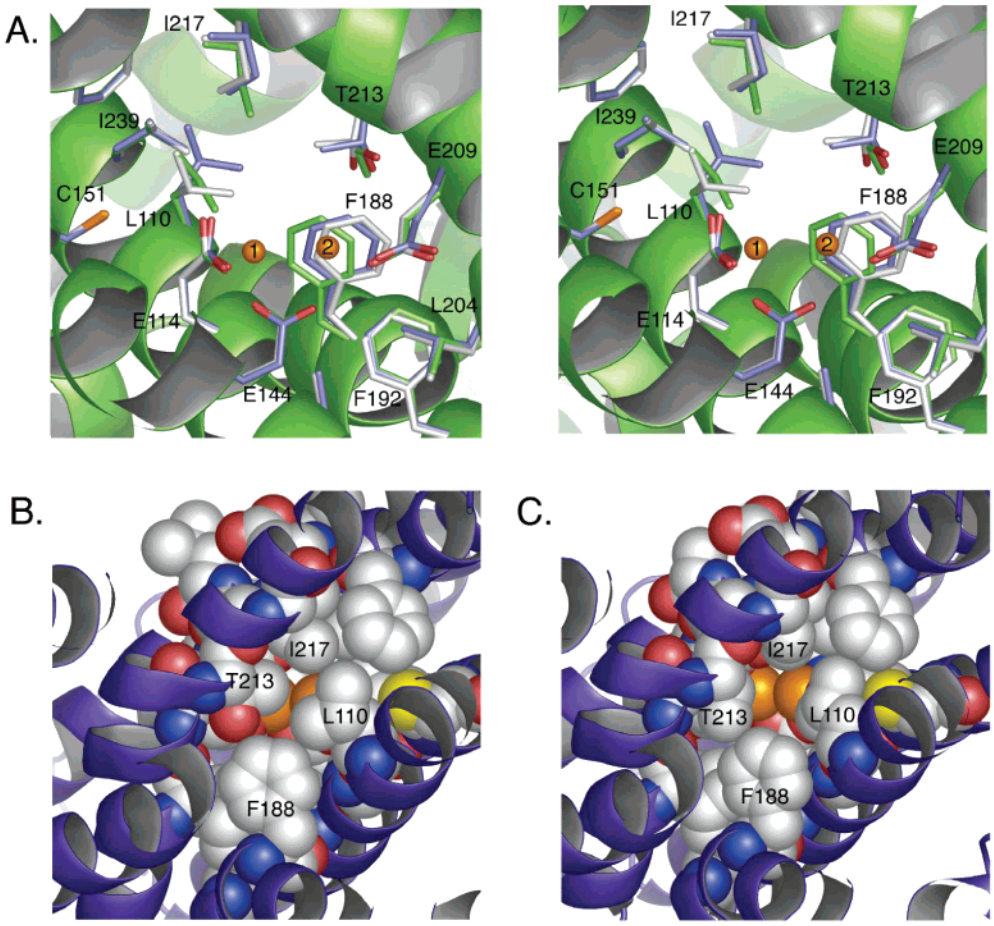

Figure 3. (A) Comparison of side-chain positions in the active site cavities of oxidized form I MMOH (gray), oxidized form II MMOH (blue), and 2-bromoethan-1-ol-bound MMOH (green), in stereoviews. The view is from behind the diiron center looking out at the leucine gate. Also shown are spacefilling representations of the leucine gate as a small molecule may approach the diiron center from cavity 2 in the (B) oxidized form I MMOH and (C) 2-bromoethan-1-ol soaked MMOH structures. Iron atoms are depicted as orange spheres. Carbon, oxygen, and nitrogen are colored as described in Figure 2. 2-Bromoethan-1-ol is not drawn in panel C.

concert with positional changes in Leu-110. Thr-213 exhibits two rotameric conformations in the product-soaked structures. In the 2-bromoethan-1-ol and 8-bromooctan-1-ol structures, the threonine hydroxyl group points toward the diiron center, whereas in the remaining bound product structures, including those with methanol and ethanol, the Thr-213 methyl group points toward the diiron center. These two different conformations have been observed previously in crystal structures of oxidized and reduced MMOH.[11,12,33,34] In some product-soaked structures, such as the one with bound 2-bromoethan-1-ol, a methyl group on the Ile-217 side chain adopts a different orientation to point toward the diiron center rather than toward Leu-110. Presumably, these conformational changes help the enzyme to accommodate better the bound products. The alternate rotameric conformations of these residues are responsible for increasing the access between cavities 1 and 2 (see below) (Figure 3B,C).

6-Bromohexan-1-ol-Induced Structural Changes in Helix E. Helix E is part of the four-helix bundle housing the diiron active site and forms one of the ridges of the canyon on the surface of MMOH. In all previously determined crystal structures of the enzyme, residues 202−211 of helix E adopt a π secondary structure, whereas the rest of its residues adopt an α-helical fold.[10−12,27,33−35] At the active site, there are three universally conserved residues, Glu-209, Thr-213, and Asn-214 on helix E. Glu-209 coordinates to the diiron center, Thr-213 forms the roof of the active site cavity and Asn-214 is positioned at the interface between the cavity and the surface above the iron-coordinating residue Glu-243. In the 6-bromohexan-1-ol bound structure, this helix, in both α-subunits of the MMOH dimer, undergoes a rearrangement in secondary structure (Figure 4). In this altered form of MMOH, residues 212−216 (FTNPL) also adopt a π-helix configuration. As a result, Thr-213 shifts to occupy the former position of Asn-214, Asn-214 shifts to occupy the former position of Pro-215, Pro-215 moves to occupy a space between its former position and that of Leu-216, and Leu-216 moves further into the active site pocket toward the leucine gate (Figures 4 and S2). At residue 217 the peptide backbone and side-chain positions resume the more typical α-helical fold. As a result of these rearrangements in MMOH, both the universally conserved Thr-213 and Asn-214 residues now lie mainly on the hydroxylase surface and the volume of cavity 1, as calculated by Swiss-PDB Viewer, increases from ∼250 to ∼330 Å^3. This volume change is primarily a result of shifting Thr-213 out, and sliding Leu-216 in, to the active site pocket, ∼5 Å behind the former position of Thr-213, replacing

(34) Rosenzweig, A. C.; Nordlund, P.; Takahara, P. M.; Frederick, C. A.; Lippard, S. J. *Chem. Biol.* **1995**, *2*, 409−418.

(35) Elango, N.; Radhakrishnan, R.; Froland, W. A.; Wallar, B. J.; Earhart, C. A.; Lipscomb, J. D.; Ohlendorf, D. H. *Prot. Sci.* **1997**, *6*, 556−568.

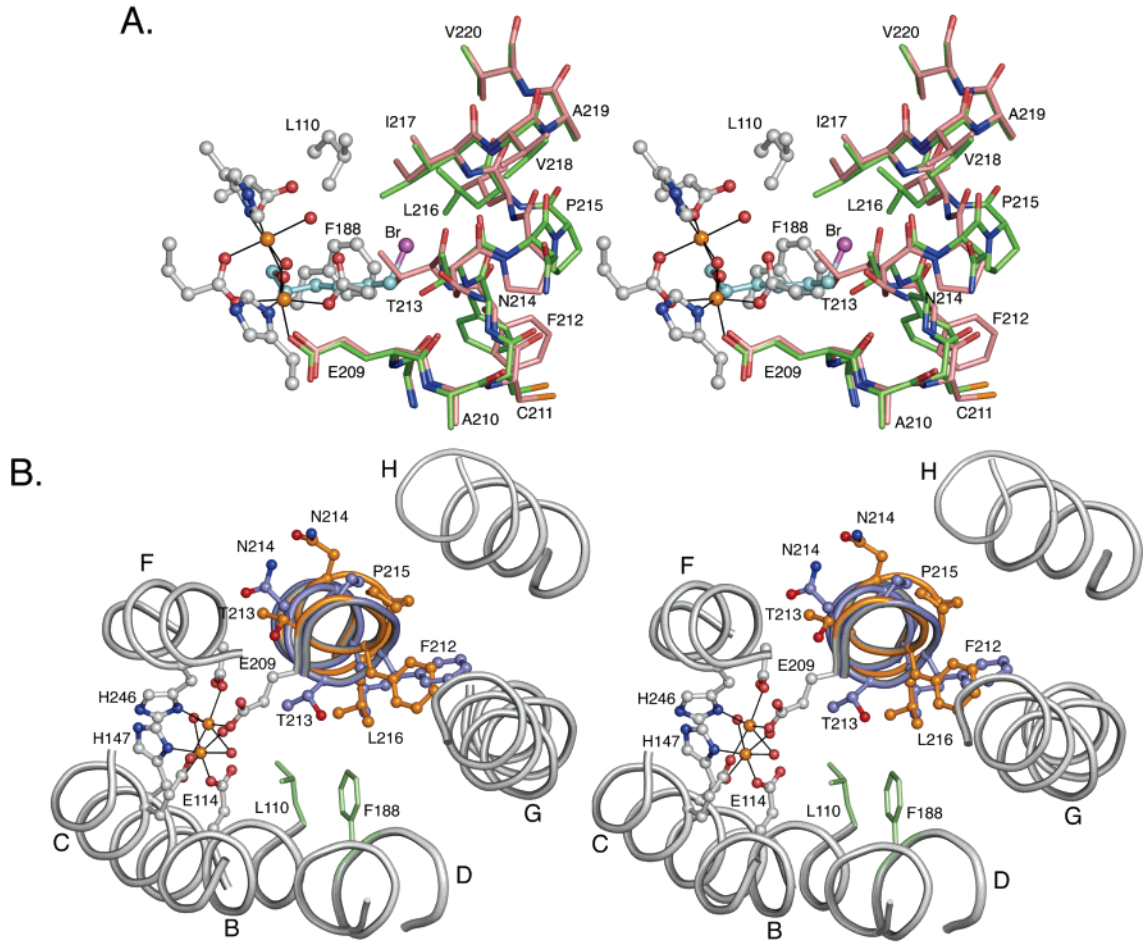

Figure 4. Structural changes in helix E of the four-helix bundle. (A) Stereoview comparing helix E from the 6-bromohexan-1-ol soaked (green) and oxidized (salmon) structures. 6-Bromohexan-1-ol (teal) is depicted to demonstrate the relative position of the bromine atom (purple) with respect to Thr-213 in oxidized MMOH. (B) Stereoview comparing active site pocket and protein surface changes due to conformational changes in helix E. Helix E of the 6-bromohexan-1-ol soaked MMOH structure is colored orange, while that of oxidized MMOH is colored blue. Helices B−H are depicted as well as leucine gate residues L110 and F188.

it as one of the residues that gates access between cavities 1 and 2. Despite the alterations in this region of the protein, the structure of the diiron center is not perturbed. Moreover, the changes within this helix do not open a pore between it and helix F of the four-helix bundle to allow direct access to the surface from the diiron center or the active site pocket. As mentioned previously, the bromine atom of 6-bromohexan-1-ol localizes to the position formerly occupied by Thr-213. It appears likely that the binding of this large product analogue to the active site cavity, and perhaps displacement of the Thr-213 side chain, induces the structural rearrangements in helix E.

X-ray data to 2.5 Å were also obtained for an MMOH crystal first soaked in 6-bromohexan-1-ol and then chemically reduced with dithionite and methyl viologen. The electron density for most of the protein is sufficiently strong to fit to a model. In both protomers the electron density in the active site is weak and, for residues 205−215, missing altogether (Figure S3). Although an exact structure of this important region cannot be determined at this time, several key observations that are relevant to the current work can be made by inspection of the electron density maps and overall B-factors of the structure (Table S1). Strong difference electron density is not observed for the bromine atom of 6-bromohexan-1-ol in the active site, indicating that reduction of the diiron center results in 6-bromohexan-1-ol leaving this region. Cavities 2 and 3, however, are occupied by this molecule since significant electron density corresponding to bromine is clearly evident (Figure S3). The absence of electron density for residues 205−215 of helix E reflects positional disorder and suggests that extrusion of 6-bromohexan-1-ol from the active site creates yet another structural reorganization in this region. Previous studies on chemically reduced MMOH crystals have not induced disorder of this magnitude near the active site cavity.[33,34]

Connectivity Between the α-Subunit Cavities. In the different product-soaked structures, the amino acid side chains separating the different cavities shift to allow access from one cavity to the next (Figure 5 and Table 3). The side chains of Leu-110, Phe-188, and Thr-213 separate cavities 1 and 2 whereas those of Phe-109, Val-285, Leu-289, and Tyr-291 separate cavities 2 and 3. In the all of the haloalkane soaked structures, cavities 2 and 3 are connected owing to a shift in the position of Leu-289 (Table 3, Figure 5B−D). This residue adopts an alternate rotameric conformation in the 8-bromooctan-1-ol-bound structure as a result of the product analogue traversing the cavity gate (Figure 5C,D). Comparisons among the other alcohol soaked structures with that of oxidized MMOH reveal that Leu-289 shifts slightly in its side-chain and backbone configuration

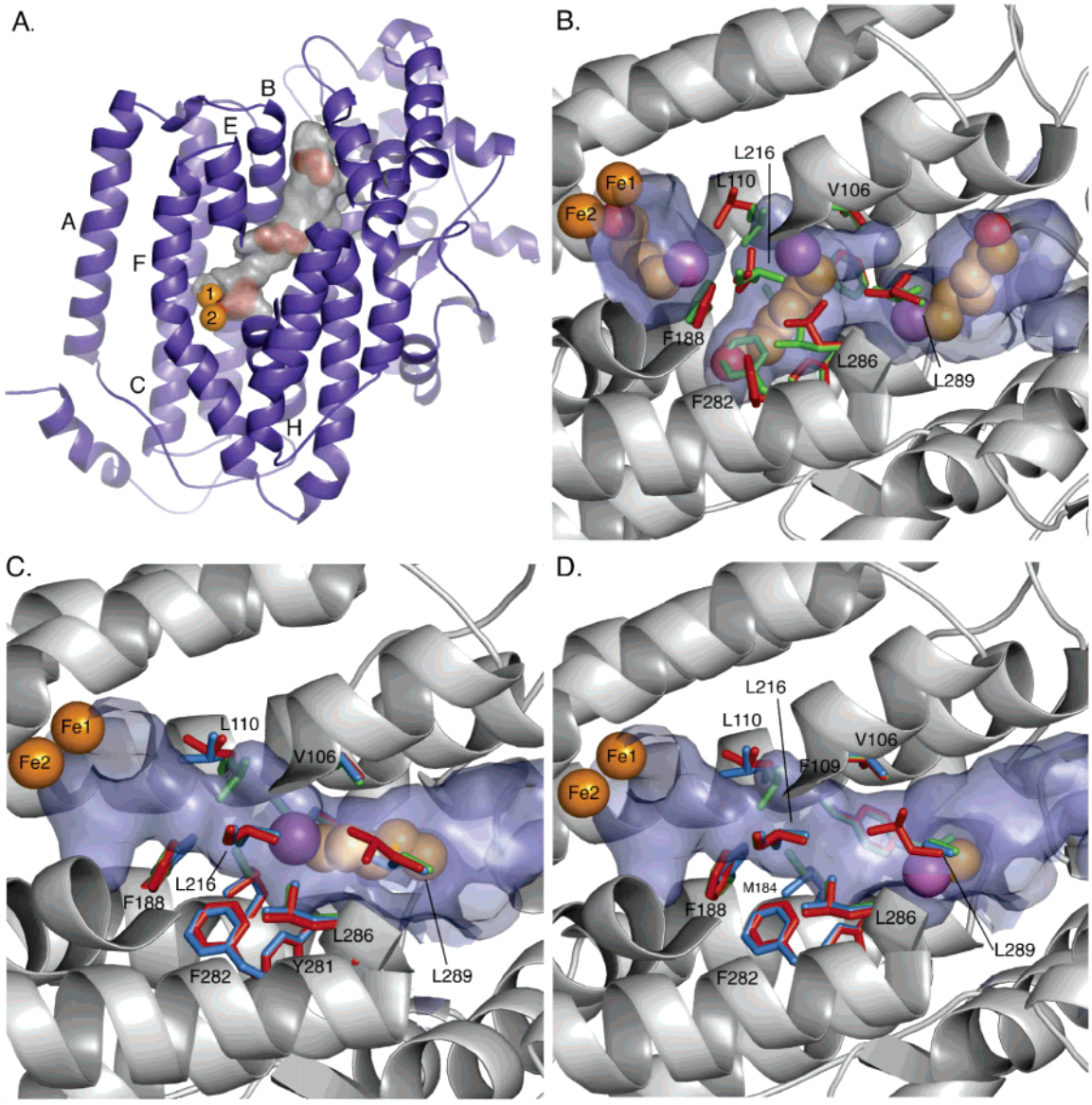

Figure 5. (A) Representation of the channel (gray) formed in the MMOH α-subunit of the 2-bromoethan-1-ol soaked structure. Parts of helices E, B, and H are cut away for better visualization. The molecules of 2-bromoethan-1-ol (red spheres) are bound as indicated in the channel. (B) Three molecules of 6-bromohexan-1-ol (spheres) bound in the α-subunit cavities (light blue). The bromine, carbon, and oxygen atoms are colored purple, yellow, and red, respectively. The positions of the cavity 2 side chains in the oxidized form II (green) and 6-bromohexan-1-ol soaked (red) MMOH structures are represented. (C, D) 8-Bromooctan-1-ol bound to the α-subunit channel (light blue) in each protamer depicting its different positions with respect to the amino acid gate, L289, between cavities 2 and 3 in the two MMOH α-subunits. 8-bromooctan-1-ol is colored as in panel B. The cavity 2 side chains for the oxidized form I (blue), oxidized form II (green), and 8-bromooctan-1-ol soaked (red) MMOH structures are identified.

to allow greater access between cavities 2 and 3 (Figure S4). The differences in the position of the Leu-289 side chain may be insignificant with respect to the connectivity between cavities 2 and 3. The distinction between these two cavities may therefore not be definitive and can vary depending on the programs used to calculate solvent accessibility. The other residues in cavity 2 adopting alternate rotameric conformations are Met-184, Phe-282, and Leu-286. Comparisons between the oxidized, 8-bromooctan-1-ol, 6-bromohexan-1-ol, and 2-bromoethan-1-ol bound structures indicate that positional changes in Phe-282 and Leu-286 are essential for MMOH to accommodate the different soaked product analogues (Figure 5B−D).

Side-chain movements in Leu-110, Phe-188, and Thr-213 of the 2-bromoethan-1-ol and 8-bromooctan-1-ol structures allow for access between cavities 1 and 2 (Figures 3 and 5). These movements, in addition to those in cavities 2 and 3, produce a ~40 Å channel leading from the diiron center to cavity 3 (Figure 5A,C). This result is the first "channel-like" occurrence in an MMOH structure. In the other product-soaked structures, which do not exhibit connectivity between cavities 1 and 2, Leu-110 and Phe-188 undergo similar positional shifts as those observed in the 2-bromoethan-1-ol and 8-bromooctan-1-ol structures. Thr-213, however, is positioned so that its hydroxyl group points toward the gates to block access between cavities 1 and 2. In the open gate configuration, the threonine hydroxyl group points toward the diiron center (Figure 3A). In the structures of reduced MMOH, in which the Thr-213 hydroxyl group is usually pointing toward the diiron center, Leu-110 and Phe-188 do not alter their positions with respect to the oxidized form to allow connectivity between the active site and cavity 2.[33,34] The change in the side-chain orientation of Thr-213 and the structural adjustments in Leu-110 and Phe-188 are therefore key to

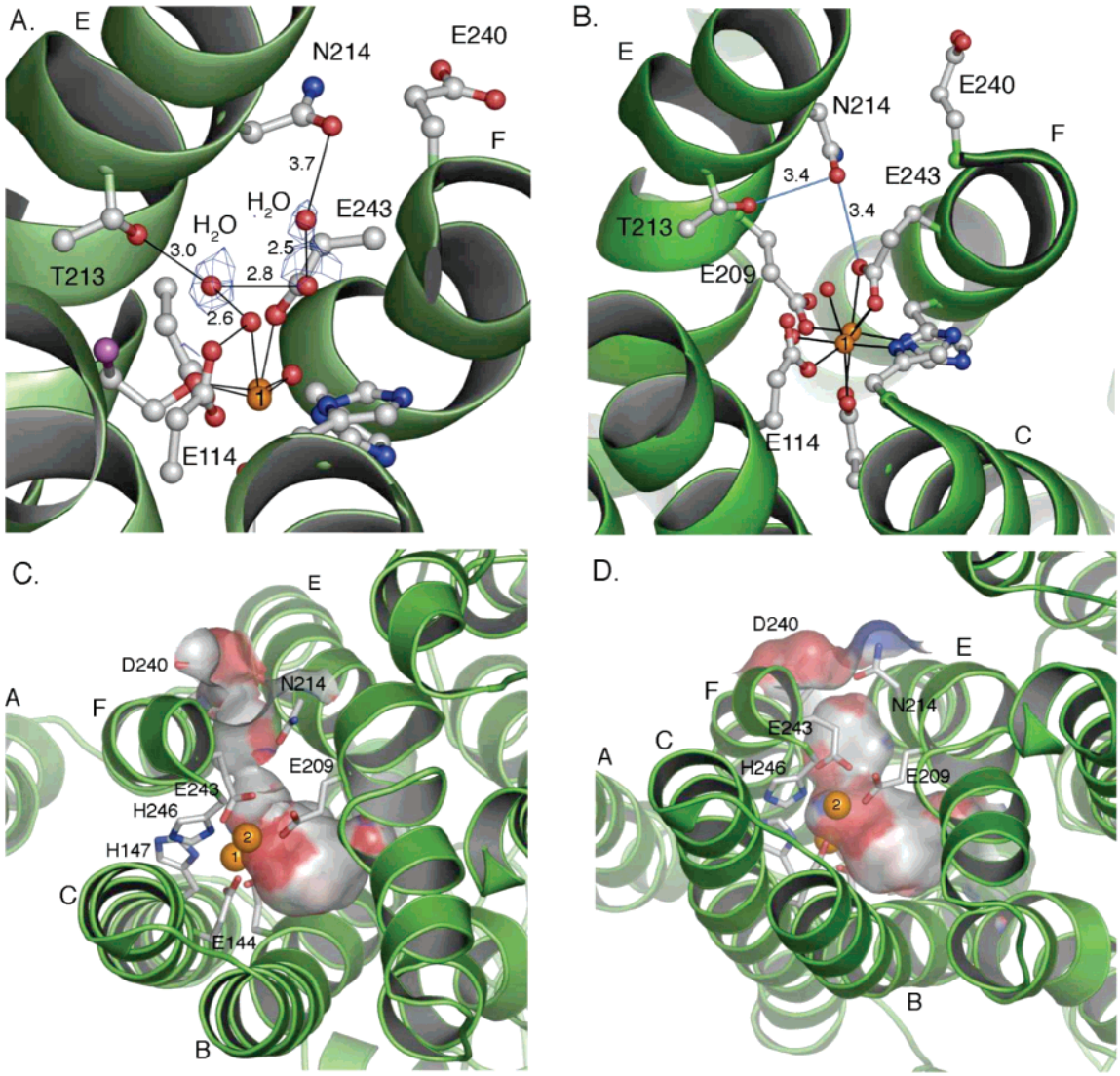

Figure 6. The effect of Asn-214 conformation on solvent accessibility to the diiron center. (A) Structure of oxidized MMOH with 2-bromoethan-1-ol bound depicting Asn-214 pointing toward solvent and novel water molecule hydrogen bonding configurations. Each water is surrounded by an $|F_o| - |F_c|$ sa-omit map contoured to 3 σ. (B) Structure of reduced MMOH in which Asn-214 points toward the diiron active site. (C) The formation of pore through the four-helix bundle of reduced MMOH demonstrating enhanced solvent accessibility as compared to (D) oxidized MMOH. All atoms are colored as described in Figure 2, and the surfaces are colored by atom type.

opening access between cavities 1 and 2. The rotameric changes in Ile-217 have no effect.

Because of these findings, cavities were calculated for the different crystal structures of MMOH in its different oxidation and small molecule bound states to track previously unassigned changes in the α-subunit. The three cavities in the oxidized, mixed-valent, methanol, ethanol, iodoethanol, dibromomethane, and xenon-bound forms differ little from one another. The structure of reduced MMOH from form I crystals exhibits slight movements in Leu-289, allowing access between cavities 2 and 3, as noted previously.[13] In reduced form II MMOH crystals, cavities 2 and 3 are connected, and cavity 1 is continuous with the MMOH surface in one protomer, indicating that molecular rearrangements have occurred to give the active site pocket direct access to solvent in the reduced state of the protein. Further analysis reveals that movement in conserved Asn-214 results in the formation of a small pore between helices E and F of the four-helix bundle that leads from the surface to the diiron center (Figure 6). In previous reduced structures, it was noticed that the movement of Asn-214 forms a deep crevice in the four-helix bundle.[36] This pore is 3.5−3.7 Å in diameter at the opening and 1.8−2.0 Å in diameter at its narrowest point. In the oxidized form of MMOH, Asn-214 shifts to close the pathway. These structural differences suggest that Asn-214 may control the entrance of small substrates such as O_2, H_3O^+, or possibly even CH_4, which have van der Waals radii of 1.52−2.15 Å, respectively, in their narrowest dimension. The presence of MMOB or protein breathing may help to widen the pore to facilitate the movement of these species into the active site.

Cavity 3, which is further removed, is formed by helices B, D, G and capped by several loops connecting the α-subunit helices. In each of the product-soaked structures, no detectable side-chain movements occur here. In no structure is the surface of this cavity contiguous with the surface of the protein.

(36) Whittington, D. A.; Lippard, S. J. *ACS Symp. Ser.* **1998**, *692*, 334−347.

Discussion

The MMOH Product-Bound State. The binding of halogenated alcohols to the bridging position of the diiron center extends previous crystallographic results demonstrating that methanol and ethanol interact with to the oxidized diiron center by displacing the bridging ligand that faces the active site pocket.[27] The geometry of the remaining iron-ligating atoms is unperturbed. These findings confirm EPR and ENDOR studies demonstrating that alcohols bind to the diiron(III) active site.[31,37] As proposed previously, the alcohol bound structures represent the final state of the enzyme, $H_{product}$, after alkane hydroxylation by Q and suggest C−H bond activation by this intermediate occurs here.[27] Density functional theory (DFT) calculations of Q reactivity with substrate are in agreement with this proposal.[38]

Conformational Changes in Helix E. Helix E is part of the α-subunit four-helix bundle that lies on the surface of MMOH near the canyon and contains within it three absolutely conserved residues, Glu-209, Thr-213, and Asn-214. In all known crystal structures of MMOH and ToMOH, residues 202−211 (190−199 ToMOH) adopt a π-helical secondary structure.[10−13,27,33−35] The binding of 6-bromohexan-1-ol to MMOH induces reorganization of this π-helix to extend it to residues 212−216, which otherwise adopt an α-helix. These unexpected geometric rearrangements in helix E are unprecedented in bacterial multicomponent monoxygenases and may have important functional implications.

One obvious consequence of the changes in helix E is that MMOH can accommodate larger molecules. The calculated volumes for cavity 1 in $MMOH_{ox}$ and the 6-bromohexan-1-ol-bound structure are ∼250 and 330 Å^3, respectively, indicating clearly that the changes provide extra space for larger substrates and products such as 6-bromohexan-1-ol. It is noteworthy, moreover, that MMOH undergoes significant reorganization in order to accommodate 6-bromohexan-1-ol binding, rather than simply excluding this product analogue from the active site, similar to what is observed for the aromatic alcohols that bind only in cavity 3. The α- to π-helical transition in residues 212−216 may be a thermodynamically downhill process, once the threshold energy for such reorganization is reached. If movement in this helix were critical to accommodate a large substrate, however, why would an enzyme designed to hydroxylate CH_4 incorporate into its fold such a reorganization mechanism unless it has another associated function?

The structural changes may represent an as-yet-unidentified effect of MMOB on the structure of MMOH. Previously, when we considered how MMOB might induce structural changes in the hydroxylase, we assumed that the effects would occur at the protein surface and translate to the diiron center. The binding of 6-bromohexan-1-ol to the MMOH active site may have triggered the reverse process, providing a glimpse of how MMOB might alter the hydroxylase structure. Only an X-ray structure of the MMOH-MMOB complex will reveal whether such an α- to π-helical change is induced by the effector protein. Nevertheless, several lines of evidence support the notion that the alterations in helix E may be physiologically relevant.

The coupling proteins in both the soluble methane monooxygenase and toluene 4-monooxygenase systems affect product regiospecificity,[39−41] and bind to helices E and F of the hydroxylase α-subunits.[42−44] To alter substrate regiospecificity, the coupling protein must in some way modulate the structure of the hydroxylase active site pocket to influence the formation of one product over another. Mutagenesis and product distribution studies of toluene 4-monooxygenase, in which conserved Thr-201 (213 in MMOH) is changed to alanine, suggest that the coupling protein alters the structure of the hydroxylase within the vicinity of this residue.[40] The rearrangements observed here for residues 212−216 on helix E of MMOH provide the first direct structural evidence supporting the hypothesis that this region of the protein can adopt more than one configuration. Furthermore, these structural changes in helix E may be responsible for the altered substrate regio- and stereospecificities in the presence of the regulatory protein, and reflect its ability to induce changes in the hydroxylase active site pocket. It is also important to note that the structural rearrangements in helix E do not perturb the geometry of the diiron center, a result that is highly consistent with numerous XAS, EPR, and Mössbauer experiments on oxidized MMOH in the presence of MMOB.[21,31,45−49]

Reduction of the 6-bromohexan-1-ol soaked MMOH crystals induces disordering of residues 205−215 and loss of the alcohol from the active site cavity. The disorder suggests the occurrence of another conformational change. Although it is unknown whether the conformation of helix E reverts to that of reduced MMOH or to a new, uncharacterized one, it appears that this helix can adopt more than one structure and may do so throughout the sMMO reaction cycle.

MMOH is not the only diiron enzyme in which helix conformational changes are observed. Helix E of class I ribonucleotide reductase (RNR−R2), like MMOH, adopts a π-helical fold in a region of the protein adjacent to its diiron center.[50−52] The structure of this helix in class Ib RNR−R2s, which occur in such species as *Salmonella typhimurium* and *Mycobacterium tuberculosis*, also exhibits two conformations, which appear to be independent of the redox state. Residues Phe-162 and Tyr-163 (*Salmonella* numbering), which are the structural analogues of Thr-213 and Asn-214 in MMOH, are repositioned to allow the diiron center greater access to solvent and O_2 from the surface of the enzyme.[51,52] These changes are

(37) Smoukov, S. K.; Kopp, D. A.; Valentine, A. M.; Davydov, R.; Lippard, S. J.; Hoffman, B. M. *J. Am. Chem. Soc.* **2002**, *124*, 2657−2663.
(38) Gherman, B. F.; Dunietz, B. D.; Whittington, D. A.; Lippard, S. J.; Friesner, R. A. *J. Am Chem. Soc.* **2001**, *123*, 3836−3837.
(39) Pikus, J. D.; Studts, J. M.; McClay, K.; Steffan, R. J.; Fox, B. G. *Biochemistry* **1997**, *36*, 9283−9289.
(40) Mitchell, K. H.; Studts, J. M.; Fox, B. G. *Biochemistry* **2002**, *41*, 3176−3188.
(41) Froland, W. A.; Andersson, K. K.; Lee, S. K.; Liu, Y.; Lipscomb, J. D. *J. Biol. Chem.* **1992**, *267*, 17588−17597.
(42) Sazinsky, M. H.; Zhu, K.; Pozharski, E.; MacArthur, R.; Riku, S.; Lippard, S. J.; Brudvig, G. W. Manuscript in preparation.
(43) MacArthur, R.; Sazinsky, M. H.; Kühne, H.; Whittington, D. A.; Lippard, S. J.; Brudvig, G. W. *J. Am. Chem. Soc.* **2002**, *124*, 13392−13393.
(44) Brazeau, B. J.; Wallar, B. J.; Lipscomb, J. D. *Biochem. Biophys. Res. Comm.* **2003**, *312*, 143−148.
(45) Fox, B. G.; Liu, Y.; Dege, J. E.; Lipscomb, J. D. *J. Biol. Chem.* **1991**, *266*, 540−550.
(46) Fox, B. G.; Hendrich, M. P.; Surerus, K. K.; Andersson, K. K.; Froland, W. A.; Lipscomb, J. D.; Münck, E. *J. Am. Chem. Soc.* **1993**, *115*, 3688−3701.
(47) Dewitt, J. G.; Rosenzweig, A. C.; Salifoglou, A.; Hedman, B.; Lippard, S. J.; Hodgson, K. O. *Inorg. Chem.* **1995**, *34*, 2505−2515.
(48) Dewitt, J. G.; Bentsen, J. G.; Rosenzweig, A. C.; Hedman, B.; Green, J.; Pilkington, S.; Papaefthymiou, G. C.; Dalton, H.; Hodgson, K. O.; Lippard, S. J. *J. Am. Chem. Soc.* **1991**, *113*, 9219−9235.
(49) Shu, L. J.; Liu, Y.; Lipscomb, J. D.; Que, L. *J. Biol. Inorg. Chem.* **1996**, *1*, 297−304.
(50) Nordlund, P.; Eklund, H. *Curr. Opin. Struct. Biol.* **1995**, *5*, 758−766.
(51) Eriksson, M.; Jordan, A.; Eklund, H. *Biochemistry* **1998**, *37*, 13359−13369.
(52) Uppsten, M.; Davis, J.; Rubin, H.; Uhlin, U. *FEBS Lett.* **2004**, *569*, 117−122.

not observed, however, in the structurally characterized class Ia RNR−R2 proteins from mouse and *Escherichia coli*.[53−55]

Inter-Cavity Gates and Molecule Movement Through MMOH. The structures of MMOH with different bound alcohols shed some light on how a small molecule might move in and out of cavity 1 at the diiron center. Previously, MMOH structures with bound substrate analogues in cavities 2 and 3,[10] and the identification of different rotameric conformations in Leu-110,[11] led to the hypothesis that the three hydrophobic α-subunit cavities may be the route for substrate entrance to the diiron center. The different product-soaked structures presented here suggest that the cavities can be used as a means of product egress as well as substrate entrance. The alternate rotameric conformations observed for those residues that form barriers between cavities 1, 2 and 3 reveal for the first time how side-chain movements can affect connectivity between the active site pocket and cavities 2 and 3 in the hydrophobic core of MMOH. In one product-soaked structure, 8-bromooctan-1-ol traverses the gate between cavities 2 and 3, outlining clearly the likely movement from one cavity to the next. Conformational changes in Thr-213, Ile-110, Phe-188, and Leu-289 are therefore likely to occur throughout the catalytic cycle to allow substrate and product passage to and from the active site.

The presence of the halogenated molecules in cavities 1−3 indicates that, in the crystalline state, MMOH is flexible enough to accommodate such product analogues. The structural changes in helix E, the cavity gates, and amino acid residues Leu-286 and Phe-282 in cavity 2 indicate how substrate accommodation may be achieved. In the active site, cavity 1, higher *B*-values and weaker electron density are the consequences of the increased size of the bound alcohol, possibly reflecting greater difficulty in passage through the α-subunit. These observations reflect trends in alkane reactivity at the diiron center reported previously,[14] where methane is the most active substrate, octane the least reactive, and the reactivities of ethane through heptane fall sequentially in between. In contrast to the halo alcohols, more rigid aromatic alcohols bind only to cavity 3, despite the fact that some of them, like phenol, bind to the diiron center in the absence of MMOB, as revealed spectroscopically.[32] These phenolic compounds are smaller than 6-bromohexan-1-ol and 8-bromooctan-1-ol and their substrate precursors, e.g., benzene, are more reactive (62 mU/mg) than either hexane or octane (9−40 mU/ mg).[14] This observation indicates that, in the crystalline state and in the absence of bound MMOB, MMOH may not be flexible enough to accommodate compounds bearing an aromatic ring. One explanation may be that MMOH is too rigid in its crystalline state to permit passage of these compounds to the active site cavity. We conclude that additional structural changes, yet to be observed, must occur to allow them access to the diiron center.

The fact that the aromatic products and 8-bromooctan-1-ol appear only in cavity 3 suggests that this region of the protein, which comprises mostly loops connecting the different α-helices, may be the initial point of entry for substrates and the final point of exit for products. The observation that all of the bound alcohols generally exhibit lower *B*-values and stronger electron density in cavity 3 than in cavities 1 or 2, lends further support to this proposal. The trend in the *B*-values is also highly consistent with data from the dibromomethane and iodoethane soaked crystals.[10]

We now address the question of how MMOB might affect the movement of molecules to and from the diiron center. MMOB alters the sMMO product distributions,[41] enhances CH_4 and O_2 reactivity with the diiron protein,[45,56] binds somewhere near helices E and F of the α-subunit four-helix bundle,[42−44] and perturbs the spectroscopic properties of the oxidized diiron(III) center when substrates such as methanol and phenol are bound.[31] Recent mutagenesis studies of Asn-202 in ToMOH, a residue analogous to Asn-214 of MMOH, reveal it to be essential for binding of its coupling protein.[57] This finding, in conjunction with chemical cross-linking and saturation recovery EPR data placing MMOB within this region, requires that the coupling protein be positioned on helix E above the diiron center. Metal reconstitution studies indicate that MMOB limits both the entry and exit of Fe^{2+} to cavity 1, possibly by decreasing α-subunit side-chain fluctuations and providing a greater barrier against solvent access.[22] An MMOB quadruple mutant containing smaller amino acids at the predicted MMOH−MMOB interface allows for enhanced reactivity of larger substrates such as furan and nitrobenzene with the diiron center.[58] Methane, however, exhibits decreased reactivity, which was attributed to quenching of the oxygenated iron intermediate by solvent. This conclusion is consistent with the solvent barrier hypothesis put forward to explain the slow rates of Fe^{2+} uptake and removal from MMOH in the presence of MMOB.[22] Moreover, deuterium isotope effects for C_2H_6 versus C_2D_6 hydroxylation are observed only when the sMMO system is reconstituted with the MMOB quadruple mutant, implying that the rate-limiting step of substrate diffusion for the reactivity of ethane with MMOH can be altered by MMOH-MMOB interactions.[59] These findings were interpreted to indicate that MMOB gates substrate access to the diiron center, presumably through the four-helix bundle, by a molecular sieving effect. The crystallographic results presented here suggest the contrary, because the apparent entrance of small molecules into the active site pocket is through the MMOH α-subunit cavities rather than directly through the four-helix bundle. So how does one rationalize these biochemical and structural data?

One possibility is that two modes of substrate entrance into cavity 1 exist. Preferred gaseous substrates such as CH_4 and O_2 may enter through the four-helix bundle, whereas the less preferred larger substrates may enter through cavity 3 and then diffuse through cavity 2 to the α-subunit to cavity 1. The primary pathway of product egress for all alcohols would be through cavities 1−3, whereas a secondary pathway could be through the four-helix bundle. The redox-dependent conformational changes of Asn-214, and the resulting formation of a pore granting solvent access to the diiron center due to these changes, imply that small molecule entry by this route may be possible. Interaction of MMOB with Asn-214 could be the trigger for

(53) Atta, M.; Nordlund, P.; Åberg, A.; Eklund, H.; Fontecave, M. *J. Biol. Chem.* **1992**, *267*, 20682−20688.
(54) Logan, D. T.; Su, X. D.; Åberg, A.; Regnström, K.; Hajdu, J.; Eklund, H.; Nordlund, P. *Structure* **1996**, *4*, 1053−1064.
(55) Strand, K. R.; Karlsen, S.; Andersson, K. K. *J. Biol. Chem.* **2002**, *277*, 34229−34238.
(56) Liu, Y.; Nesheim, J. C.; Lee, S.-K.; Lipscomb, J. D. *J. Biol. Chem.* **1995**, *270*, 24662−24665.
(57) Cadieux, E.; McCormick, M. S.; Sazinsky, M. H.; Lippard, S. J., Manuscript in preparation.
(58) Wallar, B. J.; Lipscomb, J. D. *Biochemistry* **2001**, *40*, 2220−2233.
(59) Brazeau, B. J.; Wallar, B. J.; Lipscomb, J. D. *J. Am. Chem Soc.* **2001**, *123*, 10421−10422.

O_2 gating,[56,57] possibly by inducing conformational shifts to make the overall diameter of the pore more acceptable for O_2 and CH_4 entrance into the active site, in addition to changing the properties of the dinuclear iron center.

ToMOH has an identical Asn residue that undergoes redox dependent conformational changes, exactly mimicking those found in MMOH.[13,60] However, the pathway for both toluene entrance and cresol egress is through a 40 Å channel that follows the same path through the α-subunit, as delineated by the cavities in MMOH. Despite their nearly identical diiron centers and supposedly similar mechanisms of dioxygen activation and hydrocarbon oxidation, ToMO is 20 times more reactive toward aromatics than sMMO,[13,14] perhaps reflecting better substrate access. Since the regulatory protein enhances O_2 reactivity in the ToMO system, as it does for sMMO, the most logical explanation that preserves a common mechanism for the two enzyme systems is that the four-helix bundle opening is a point of entry for a small molecule. We suggest that this species could be the proton, or H_3O^+, and that a function of MMOB might be to exclude protonation of the H_{peroxo} and Q catalytic intermediates so that they can react with substrates. Dissociation of MMOB would then occur after product release to allow proton-coupled electron transfer as the oxidized enzyme is reduced to the diiron(II) state to initiate another round of catalysis. Another possibility is that MMOB gates dioxygen access through this route. The present crystallographic data suggest that the cavities in MMOH may represent the major route of product exit. The question of how small molecules move through BMMs will best be clarified by detailed mutagenesis studies on the hydroxylase component and by obtaining a crystal structure of the hydroxylase-regulatory protein complex.

Why Cavities? The structures of MMOH with bound substrate and product analogues outline a clear pathway by which some small molecules may move through the α-subunit. The "open cavity" or "channel-like" conformation observed in the 2-bromoethan-1-ol and 6-bromohexan-1-ol structures is remarkably similar to that of the channel in toluene monooxygenases, which gives the diiron center in these BMMs unimpeded access to the protein surface.[13] The major structural difference between the sMMO and TMO hydroxylase components is the greater solvent access in the latter. It has been hypothesized that solvent access may be responsible for the differential methane reactivity in the sMMO and TMO systems.[13] For an aromatic hydroxylating protein, methane may be too small a substrate to block solvent access from the channel. In contrast, aromatic compounds, when docked into the ToMO active site pocket, can reliably function in this manner (Figure S5), thereby keeping the active oxygen intermediates from being quenched by buffer components. For sMMO, the cavity gates and MMOB (vide supra), may similarly function to block solvent access to the interior of the protein (Figure 3B) and to facilitate reactivity of methane with the dioxygen-activated diiron center. If true, the presence of cavities in sMMO may be absolutely essential to its function.

Several studies of dioxygen-utilizing iron proteins have demonstrated the importance of protecting a redox active metal from solvent as a means of preserving the activity of the protein. Myohemerythrin and hemerythrin are members of the carboxylate-bridged diiron center family of proteins that function to transport dioxygen in marine invertebrates. Mutagenesis studies on a conserved leucine reside that was proposed previously to gate O_2 entrance into the hydrophobic active site indicate that the size and shape of this residue are required to gate solvent access to the diiron center and limit autoxidation.[61,62] Similarly, the dioxygen-coordinating face of the heme moiety in hemoglobin and myohemoglobin is buried within the interior of the protein. Solvent access to this center inactivates the protein by oxidation of the heme to the ferric state.[63] The principle of solvent exclusion, although not a new one in bioinorganic chemistry, may not have received proper consideration in our understanding of BMMs. Protection of the diiron center may be achieved in two ways. As demonstrated by stopped-flow studies on sMMO from *M. trichosporium* (OB3b) using the MMOB quadruple mutant,[58] and by metal reconstitution studies of MMOH from *M. capsulatus* (Bath),[22] binding of the effector protein is one method by which the enzyme system limits solvent and substrate access to the diiron center directly through the four-helix bundle. The use of cavities and channels in the hydroxylase α-subunit is the other manner in which solvent movement may be controlled. For sMMO and ToMO, the principle of solvent exclusion may be the key to the differences in substrate reactivity between the two enzymes and their families.

Acknowledgment. This research was supported by NIGMS Grant GM32134. M.H.S. was an NIH Biotechnology grant trainee. We thank Lisa Chatwood, Yongwon Jung, Dan Kopp, Mike McCormick, and Adam Silverman for assistance with data collection and processing.

Supporting Information Available: Table S1 comparing B-factors between the different MMOH structures and Figures S1, S2, S3, S4, and S5, depicting the locations of bound products and side-chain differences between some MMOH structures. This material is available free of charge via the Internet at http://pubs.acs.org. See any current masthead page for ordering information and Web access instructions.

JA044099B

(60) McCormick, M. S.; Sazinsky, M. H.; Lippard, S. J. Unpublished results (2004).

(61) Farmer, C. S.; Kurtz, D. M., Jr.; Phillips, R. S.; Ai, J.; Sanders-Loehr, J. *J. Biol. Chem.* **2000**, *275*, 17043−17050.

(62) Raner, G. M.; Martins, L. J.; Ellis, W. R., Jr. *Biochemistry* **1997**, *36*, 7037−7043.

(63) Stryer, L. *Biochemistry*, 4th ed.; W. H. Freeman and Company: New York, 1995.